ZYG-12/Hook's dual role as a dynein adaptor for early endosomes and nuclei is regulated by alternative splicing of its cargo binding domain

Cátia Carvalho[a,b,c,#], Matilde Moreira[a,b,#], Daniel J. Barbosa[a,b,d], Fung-Yi Chan[a,b], Carlota Boal Koehnen[a,b], Vanessa Teixeira[a,b,c,], Helder Rocha[a,b,e], Mattie Green[f], Ana Xavier Carvalho[a,b], Dhanya K. Cheerambathur[f], and Reto Gassmann[a,b,*]

[a]i3S – Instituto de Investigação e Inovação em Saúde, Universidade do Porto, 4200-135 Porto, Portugal; [b]IBMC – Instituto de Biologia Molecular e Celular, 4200-135 Porto, Portugal; [c]ICBAS – Instituto de Ciências Biomédicas Abel Salazar, Universidade do Porto, 4050-313 Porto, Portugal; [d]1H-Toxrun – One Health Toxicology Research Unit, University Institute of Health Sciences, CESPU, CRL, 4585-116 Gandra, Portugal; [e]ATC de Anatomia Patológica, Citológica e Tanatológica, Escola Superior de Saúde, Instituto Politécnico do Porto, 4200-075 Porto, Portugal; [f]Institute of Cell Biology, School of Biological Sciences, University of Edinburgh, Edinburgh EH9 3BF, United Kingdom

ABSTRACT **The microtubule motor cytoplasmic dynein-1 transports and positions various organelles, but the molecular basis of this functional diversity is not fully understood. Cargo adaptors of the Hook protein family recruit dynein to early endosomes (EE) in fungi and human cells by forming the FTS–Hook–FHIP (FHF) complex. By contrast, the *Caenorhabditis elegans* Hook homologue ZYG-12 recruits dynein to the nuclear envelope (NE) in the meiotic gonad and mitotic early embryo by forming a Linker of Nucleoskeleton and Cytoskeleton (LINC) complex. Here, we demonstrate that ZYG-12 recruits dynein to EE in epithelia. We identify and functionally characterize the homologues of FTS (UBC-19) and FHIP (FHIP-1) that constitute the *C. elegans* FHF complex, validate the predicted FHIP-1–RAB-5 binding interface in vivo, and show that ZYG-12 forms FHF via a conserved segment that precedes, and is distinct from, its C-terminal NE targeting domain. Finally, we show that C-terminal ZYG-12 splice isoforms differ in their ability to target to the NE and EE. We conclude that the *C. elegans* Hook adaptor evolved to recruit dynein to two distinct organelles, and that cargo specificity of ZYG-12 is regulated by alternative splicing.**

SIGNIFICANCE STATEMENT

- The microtubule motor cytoplasmic dynein-1 transports a multitude of cargos, but the molecular basis of this functional diversity is not fully understood.
- The authors show that *C. elegans* ZYG-12/Hook forms two distinct complexes to recruit dynein to early endosomes and the NE, and that this dual role of the adaptor is regulated in a tissue-specific manner by alternative splicing of its C-terminal cargo binding domain.
- The characterization of the *C. elegans* FTS–Hook–FHIP complex provides molecular insight into dynein recruitment to early endosomes in animals and reveals alternative splicing as a mechanism to regulate cargo specificity of dynein adaptors.

Monitoring Editor
Needhi Bhalla
University of California, Santa Cruz

Received: Sep 3, 2024
Revised: Dec 6, 2024
Accepted: Dec 21, 2024

New Hypothesis

New Materials

INTRODUCTION

As the major microtubule minus end-directed motor, cytoplasmic dynein-1 (dynein) is critical for numerous cellular processes, including organelle positioning, endocytic and exocytic trafficking, mitotic spindle assembly, and maintenance of cell polarity. The dynein complex is built around a single type of heavy chain motor subunit (DHC) and requires adaptor proteins for recruitment to its diverse cargo (Reck-Peterson *et al.*, 2018). Because the number of dynein cargos surpasses the number of adaptors, some adaptors have evolved to recognize more than one type of cargo (Reck-Peterson *et al.*, 2018), raising the question of how cargo specificity is regulated.

Activating adaptors are dimeric coiled-coil proteins with a bipartite architecture: the N-terminal region forms a complex with dynein and its obligatory cofactor, the dynactin complex, while the C-terminal region links to cargo (Carter *et al.*, 2016). The processive transport machine containing the adaptor N-terminal region forms through interactions that are similar across different adaptor families. One universally conserved interaction involves the binding of a dynein light intermediate chain (DLIC) C-terminal helix to the adaptor N-terminus as it emerges from the dynactin filament (Lee *et al.*, 2018). On the adaptor side, the DLIC helix can be accommodated by different N-terminal domains, including the Hook domain that defines the Hook adaptor family described below.

In contrast to the overall similar structure of dynein–dynactin–adaptor assemblies, adaptor–cargo interactions are more divergent. The Hook family of activating adaptors binds cargo in the context of the FTS–Hook–FHIP (FHF) complex (Xu *et al.*, 2008), which in addition to the Hook dimer contains one copy each of the proteins FTS (an E2 ubiquitin-conjugating enzyme variant) and FHIP. In human cells, three Hook paralogues (HOOK1–3) form combinatorial complexes with four FHIP paralogues (FHIP1A, 1B, 2A, 2B), which in turn interact with different membrane cargo, including early endosomes (EE), ER-to-golgi vesicles, and mitochondria (Christensen *et al.*, 2021). The FTS–HOOK1/3–FHIP1B complex is recruited to EE through a direct interaction between FHIP1B and GTP-bound Rab5 (Christensen *et al.*, 2021). The structure of human FHF, recently determined by cryo-EM (Abid Ali *et al.*, 2025), shows that the HOOK3 C-terminus is buried within FTS and FHIP1B, while the opposing side of FHIP1B is predicted to interact with Rab5. Work in the filamentous fungi *A. nidulans* and *U. maydis*, which express one homologue each of FTS, Hook and FHIP, has shown that FHF is critical for dynein-mediated EE transport (Bielska *et al.*, 2014; Yao *et al.*, 2014; Zhang *et al.*, 2014).

Caenorhabditis elegans ZYG-12 was the first Hook protein implicated in dynein recruitment (Malone *et al.*, 2003). In contrast to its vertebrate and fungal homologues, ZYG-12 contains a C-terminal transmembrane domain followed by a KASH motif, which mediates targeting to the nuclear envelope (NE) (Figure 1A; Malone *et al.* 2003). In the perinuclear space, the KASH motif binds the protein SUN-1, which in turn traverses the inner nuclear membrane to complete the bridge between cytoplasm and nucleoplasm (Minn *et al.*, 2009). In the meiotic gonad, the Linker of Nucleoskeleton and Cytoskeleton (LINC) complex formed by this SUN/KASH pair transmits forces that move chromosomes, facilitate homologue pairing, and prevent nonhomologous synapsis (Penkner *et al.*, 2007, 2009; Sato *et al.*, 2009). ZYG-12–mediated recruitment of dynein to the NE is also required to maintain syncytial gonad architecture and keep centrosomes attached to the nucleus in the dividing early embryo (Malone *et al.*, 2003; Zhou *et al.*, 2009). Consequently, ZYG-12 inhibition causes severe meiotic and mitotic chromosome mis-segregation and is embryonically lethal (Malone *et al.*, 2003). Whether ZYG-12 has functions beyond cell division is unknown.

Here, we show that, in epithelia, ZYG-12 functions as part of the FHF complex. Deleting a conserved ZYG-12 segment that precedes the C-terminal NE targeting domain and is predicted to bind UBC-19 (FTS) and FHIP-1 abrogates ZYG-12 recruitment to EE without perturbing LINC complex function. FHIP-1 is strictly required for ZYG-12 recruitment to EE, whereas UBC-19 only becomes essential when the FHIP-1 binding motif in ZYG-12 is mutated. We also show that ZYG-12 recruitment to EE and the NE is regulated by alternative splicing of its C-terminal region. Our study delineates molecular determinants governing dynein recruitment to EE in animals and reveals alternative splicing of adaptors as a mechanism to regulate the specificity of dynein–cargo interactions.

RESULTS

The Hook domain protein ZYG-12 recruits dynein to the nuclear envelope and early endosomes in a tissue-specific manner

The sole *C. elegans* Hook domain protein ZYG-12 forms a LINC complex with SUN-1 at the NE (Figure 1A). To determine whether ZYG-12 function is restricted to the NE, we tagged endogenous ZYG-12 with GFP and examined its subcellular localization in different tissues. In the embryo, GFP::ZYG-12 localized to the NE and was additionally enriched around mitotic centrosomes (Malone *et al.*, 2003), presumably reflecting its localization to ER membrane that also contains SUN-1, referred to as the centriculum (Maheshwari *et al.*, 2023) (Figure 1B). In the meiotic hermaphrodite gonad, GFP::ZYG-12 also localized to the NE, where it formed prominent patches in the transition zone that colocalized with endogenous mCherry-tagged DHC-1 (Figure 1C). These patches reflect the association of the LINC complex with chromosomal regions that promote pairing and synapsis (Sato *et al.*, 2009). In contrast to the gonad and early embryo, GFP::ZYG-12 was absent from the NE in the epidermal hyp7 and seam syncytia and instead colocalized with mCh::DHC-1 in cytoplasmic puncta (Figure 1C). mCh::DHC-1 was delocalized in the DLI-1(F392A/F393A) mutant (Figure 1, D and E), which prevents the DLIC C-terminal helix from binding to adaptor N-termini (Celestino *et al.*, 2019), suggesting that dynein recruitment to cytoplasmic GFP::ZYG-12 puncta requires the interaction between DLI-1 and the ZYG-12

This article was published online ahead of print in MBoC in Press (http://www.molbiolcell.org/cgi/doi/10.1091/mbc.E24-08-0364) on December 24, 2024.

[#]These authors contributed equally to this work.

Author contributions: C.C. and R.G. conceived and designed the experiments; C.C., M.M., D.J.B., F.-Y.C., V.T., H.R., M.G., D.K.C., and R.G. performed the experiments; C.B.K. and M.M. analyzed the data; R.G. drafted the article; R.G. prepared the digital images; A.X.C. resources & experimental advice.

Conflict of interest: The authors declare no financial conflicts of interest.

*Address correspondence to: Reto Gassmann (rgassmann@ibmc.up.pt).

Abbreviations used: CI, confidence interval; DHC, dynein heavy chain; DIC, differential interference contrast; DLIC, dynein light intermediate chain; EE, early endosome(s); ER, endoplasmic reticulum; FHF, FTSHookFHIP; FHIP, FTS/Hook Interacting Protein; FTS, Fused Toes; GFP, green fluorescent protein; ko, knockout; mCh, mCherry; NE, nuclear envelope; NEBD, nuclear envelope breakdown; TM, transmembrane; VPC, vulval precursor cell; wt, wild-type.

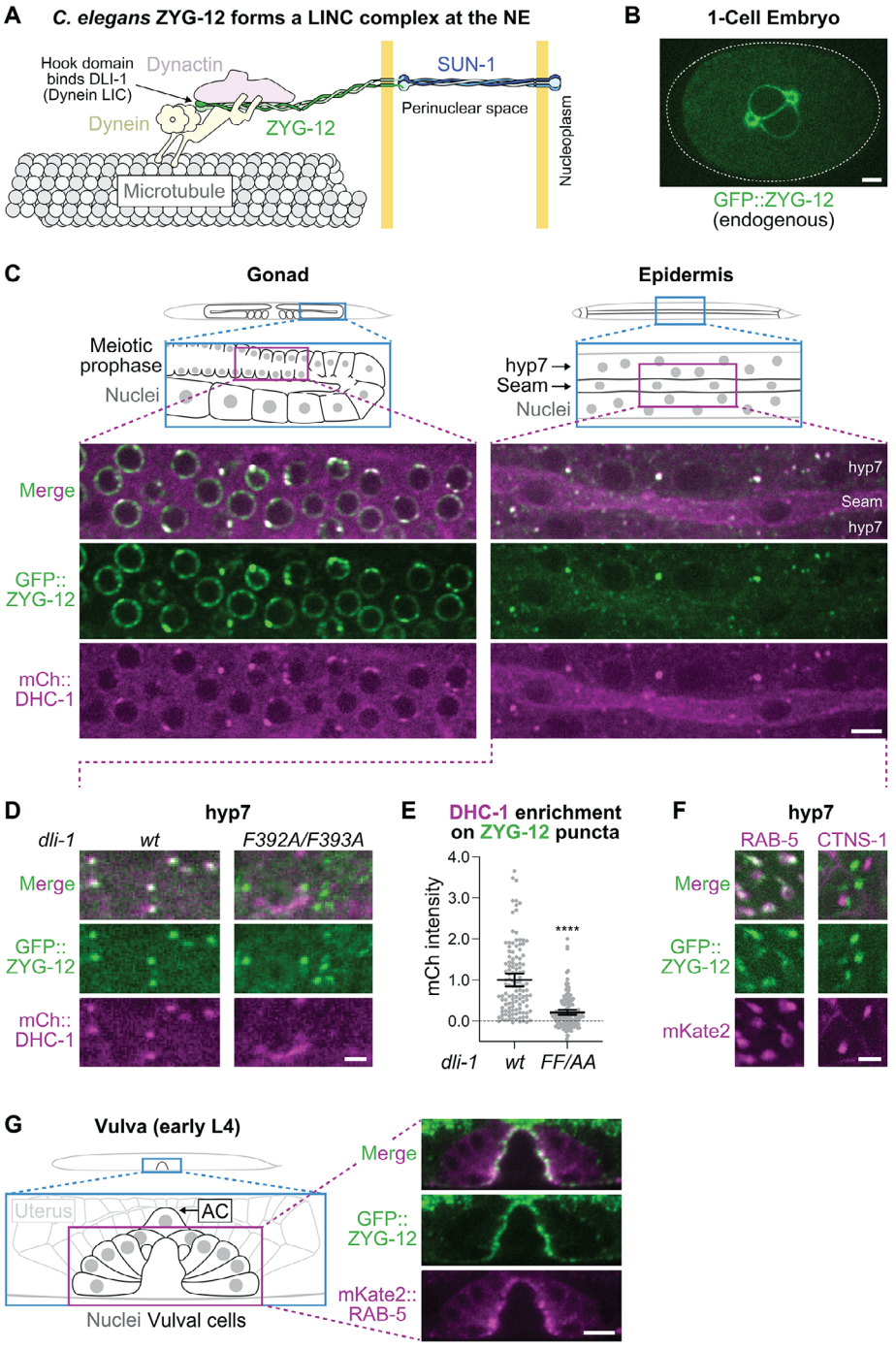

FIGURE 1: The Hook domain protein ZYG-12 recruits dynein to the nuclear envelope and early endosomes in a tissue-specific manner. (A) Schematic illustrating ZYG-12's role in dynein recruitment to the nuclear envelope through formation of a LINC complex with SUN-1. (B) Image of a one-cell embryo just prior to NEBD expressing endogenously tagged GFP::ZYG-12. Scale bar, 5 µm. (C, D) Images of the gonad and epidermis in L4 animals coexpressing GFP::ZYG-12 and endogenously tagged mCherry::DHC-1 (dynein heavy chain). *wt*, wild-type. Scale bars, 5 µm (C) and 2 µm (D). (E) mCherry::DHC-1 intensity on GFP::ZYG-12 puncta in hyp7, quantified in images such as (D). Measurements of individual puncta from at least 10 animals are shown along with mean ± 95% CI (total number of puncta = 119 and 154 for *wt* and *FF/AA*, respectively). Statistical significance was determined by the Mann–Whitney test. ****$P < 0.0001$. CI, confidence interval. (F) Images of hyp7 in L4 animals coexpressing GFP::ZYG-12 and transgenic mKate2-tagged probes for EE (RAB-5) or lysosomes (CTNS-1). Similar results were observed in at least 10 animals for each condition. Scale bar, 2 µm. (G) Image of the developing vulva in an early L4 animal coexpressing GFP::ZYG-12 and transgenic mKate2::RAB-5. AC, anchor cell. Scale bar, 5 µm.

Hook domain. Epidermal GFP::ZYG-12 colocalized with transgenic mKate2::RAB-5 but not CTNS-1::mKate2 (a marker for lysosomes) (Figure 1F), revealing that the cytoplasmic ZYG-12 puncta correspond to EE. Aside from the larval epidermis, GFP::ZYG-12 also localized to cytoplasmic puncta (but not to the NE) in the intestine, rectum, and the developing uterus and vulva (Figure 1G; Supplemental Figure S1, A and B). In these epithelia, GFP::ZYG-12 puncta were predominantly concentrated on the apical side. Expression of transgenic mKate2::RAB-5 in the L4-stage vulva revealed prominent apical enrichment of this marker (Figure 1G; Supplemental Figure S1B), suggesting that the polarized distribution of GFP::ZYG-12 reflects its association with EE. Taken together, these results show that ZYG-12 localizes to two distinct organelles and indicate that this dual function of the dynein adaptor is regulated in a tissue-specific manner.

FHIP-1 recruits ZYG-12 to early endosomes but is dispensable for ZYG-12 function at the nuclear envelope

ZYG-12's localization to EE suggested that it does so in the context of the FHF complex, as described for Hook proteins in vertebrates and fungi (Figure 2A). Sequence searches identified the uncharacterized proteins UBC-19 and C05D11.8 as the likely homologues of the FHF subunits FTS and FHIP, respectively. Like FTS homologues in other species, UBC-19 contains an ubiquitin E2 variant domain (entry cd23814 in the conserved protein domain database; https://www.ncbi.nlm.nih.gov/Structure/cdd/cdd.shtml; Wang *et al.*, 2022). C05D11.8 was already annotated in WormBase as an FHIP family protein and is hereafter referred to as FHIP-1.

Insertion of GFP into an internal loop of FHIP-1 revealed colocalization with mKate2::RAB-5 in the larval epidermis (Figure 2B), whereas no GFP signal was detectable in the gonad and early embryo (Supplemental Figure S1C). To probe the function of FHIP-1, we generated a knockout (*ko*), which was fully viable and fertile (Supplemental Figure S1D). In *fhip-1(ko)* animals, GFP::ZYG-12 was absent from epidermal mKate2::RAB-5 puncta (Figure 2, C and D) but localized normally to the NE in the gonad and one-cell embryo (Figure 2E). Furthermore, L4 *fhip-1(ko)* animals lacked the polarized apical localization of GFP::ZYG-12 in the developing vulva (Figure 2F). Immunoblotting confirmed that total GFP::ZYG-12 levels are unaffected by *fhip-1(ko)* (Supplemental Figure S1E). We conclude that FHIP-1 is required for ZYG-12 recruitment to EE but dispensable for ZYG-12 function at the NE. This demonstrates that ZYG-12 recruitment to the two organelles involves distinct mechanisms.

Structure prediction identifies FHIP-1 residues important for recruitment to RAB-5

Prior work on the human FHF complex showed that FHIP1B binds to GTP–Rab5 (Christensen *et al.*, 2021). To gain molecular insight into this interaction, we used AlphaFold 3 (AF3) (Abramson *et al.*, 2024) to predict the structure of FHIP-1 in complex with GTP–RAB-5 and mutated three surface-exposed FHIP-1 residues at the predicted binding interface (Figure 3A). G282 and A285 were mutated to the bulkier glutamine, and R292 was mutated to glutamate to reverse charge ("QQE" mutant). Immunoblotting showed that the GFP-tagged FHIP-1 mutant is expressed, albeit at reduced levels (Supplemental Figure S1E). FHIP-1(QQE)::GFP was mostly delocalized from epidermal mKate2::RAB-5 puncta (Figure 3, B and C) and no longer exhibited polarized localization in the L4 vulva (Figure 3D). These results support the idea that the mutated FHIP-1 residues form part of the RAB-5 binding interface.

ZYG-12 recruitment to early endosomes and the nuclear envelope is mediated by distinct C-terminal domains

Further structure prediction analysis suggested that RAB-5 and ZYG-12/UBC-19 interact with FHIP-1 on opposite sides (Supplemental Figure S2A), in agreement with the recently determined cryo-EM structure of human FHF (Abid Ali *et al.*, 2025). The ZYG-12 region predicted to interact with FHIP-1 and UBC-19, referred to here as the FHF domain, is located just before a flexible linker that in turn precedes the transmembrane domain and KASH motif (Figure 4A). To determine the functional relevance of ZYG-12's FHF domain, we deleted residues 686–730, leaving the linker, transmembrane domain, and KASH motif intact. Similar to what we observed in *fhip-1(ko)* animals, GFP::ZYG-12(Δ686–730) was largely absent from epidermal mKate2::RAB-5 puncta (Figure 4, B and C) but localized normally to the NE in the gonad and one-cell embryo (Figure 4D). Mutant animals were fully viable and fertile (Supplemental Figure S1D), and immunoblotting confirmed robust overall expression of the mutant (Supplemental Figure S1E). We conclude that *zyg-12(Δ686–730)* is a separation-of-function mutant that selectively perturbs ZYG-12 recruitment to EE.

The FTS homologue UBC-19 becomes essential for ZYG-12 recruitment to early endosomes when the FHIP-1 binding site in ZYG-12 is mutated

The FHF domain of human HOOK3 makes distinct contacts with FTS and FHIP1B (Abid Ali *et al.*, 2025). FHIP1B binding is mediated by a short helical segment at the C-terminus of the FHF domain, which is highly conserved among Hook proteins, including ZYG-12 (Figure 4A). Consistent with this, AF3 predicts the interaction between the ZYG-12 helix and FHIP-1 with high confidence (Supplemental Figure S2B). To determine the functional importance of this interaction, we mutated all of the conserved residues in the ZYG-12 helix to alanine (6A mutant; Figure 4A). Unexpectedly, GFP::ZYG-12(6A) localized normally to epidermal mKate2::RAB-5 puncta (Figure 4, E and F) and exhibited robust polarized localization in the vulva of L4 animals (Figure 4G). These results suggested that ZYG-12 can be recruited to EE without directly binding to FHIP-1, which prompted us to examine the role of UBC-19. In a *ubc-19(ko)* background, wild-type GFP::ZYG-12 was partially delocalized, while the GFP::ZYG-12(6A) mutant largely failed to localize, essentially mimicking the effect of Δ686–730 (Figure 4, E–G). We conclude that while FHIP-1 is strictly required for ZYG-12 recruitment to EE, UBC-19 plays a more auxiliary role. In the human FHF structure (Abid Ali *et al.*, 2025) and the predicted structure of *C. elegans* FHF (Supplemental Figure S2A), FTS wraps around Hook, thereby tethering it to FHIP. The role of UBC-19 as a seat belt for ZYG-12 may explain why mutating the ZYG-12 helix does not perturb ZYG-12 recruitment to EE as long as UBC-19 is present.

FHF inhibition affects early endosome distribution in vulval precursor cells

We next used the *fhip-1(ko)* and *zyg-12(Δ686–730)* mutants to assess the importance of FHF for EE distribution. At the larval L3 stage, vulval precursor cells (VPCs) exhibited enrichment of mKate2::RAB-5 puncta on their apical side (Supplemental Figure S3A), which was less pronounced in *fhip-1(ko)* and *zyg-12(Δ686–730)*. The arrangement of VPCs in a single row facilitated quantification of EE distribution by line scan analysis along the apical-basal axis, which confirmed a decrease, albeit modest, in apical mKate2::RAB-5 signal in the mutants (Supplemental Figure S3B). We also assessed dynein-mediated EE movements

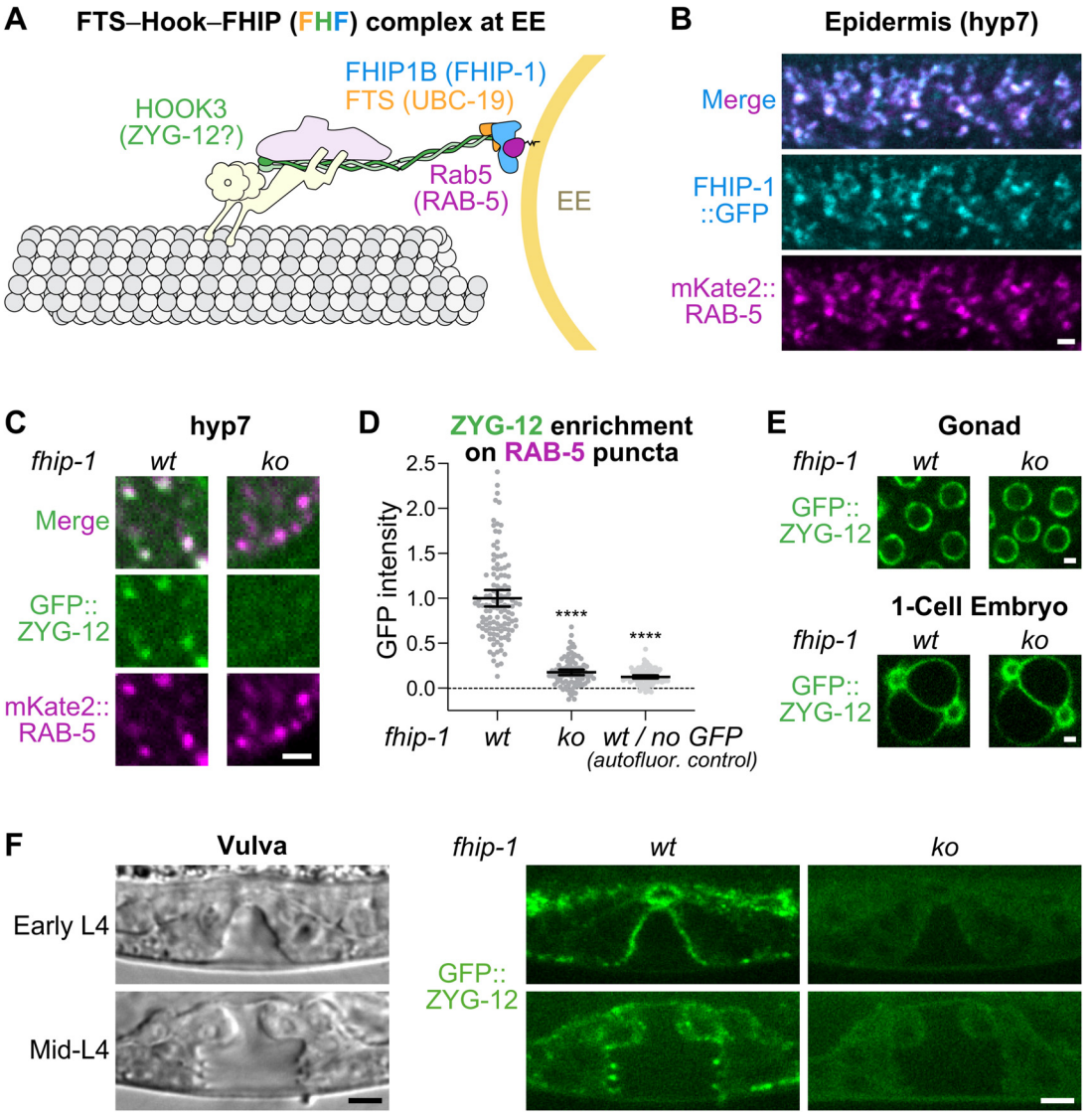

FIGURE 2: The *C. elegans* FHIP homologue recruits ZYG-12 to early endosomes but is dispensable for ZYG-12 function at the nuclear envelope. (A) Schematic of the human FHF complex recruited to EE by Rab5. Names of *C. elegans* homologues are in brackets. (B) Image of hyp7 in an L4 animal coexpressing endogenously tagged FHIP-1::GFP and transgenic mKate2::RAB-5. Scale bar, 2 µm. (C) Images of hyp7 in L4 animals coexpressing GFP::ZYG-12 and transgenic mKate2::RAB-5. *wt*, wild-type; *ko*, knockout. Scale bar, 2 µm. (D) GFP::ZYG-12 intensity on mKate2::RAB-5 puncta in hyp7, quantified in images such as (C). Measurements of individual puncta from at least 10 animals are shown along with mean ± 95% CI (total number of puncta = 118, 98, and 99 for *wt*, *ko*, and *ko/no GFP*, respectively). Untagged ZYG-12 was included as a control for autofluorescence when imaging in the GFP channel. Statistical significance was determined by ANOVA on ranks (Kruskal–Wallis nonparametric test) followed by Dunn's multiple comparison test. ****$P < 0.0001$. CI, confidence interval. (E) Images of GFP::ZYG-12 in the L4 meiotic gonad and one-cell embryo. Similar localization was observed in gonads and embryos of at least 10 animals for each condition. Scale bars, 2 µm. (F) Differential interference contrast (DIC) and fluorescence images of the L4 vulva in animals expressing GFP::ZYG-12. DIC images on the left correspond to the *wt* fluorescence images on the right. Similar localization was observed in at least 10 animals for each condition and developmental stage. Scale bars, 5 µm.

toward mitotic centrosomes during the first embryonic division (Kimura and Kimura, 2011; Barbosa *et al.*, 2017). EE movements were still observed in *fhip-1(ko)* embryos (Supplemental Figure S3C), consistent with the absence of detectable FHIP-1::GFP expression at this developmental stage (Supplemental Figure S1C). These observations suggest that FHF contributes to the polarized EE distribution in VPCs, whereas FHF is dispensable for centrosome-directed EE motility in the early embryo.

ZYG-12 recruitment to early endosomes and the nuclear envelope is regulated by C-terminal splicing

In addition to the full-length ZYG-12 isoform B that contains the FHF domain (encoded by exons 6 and 7), a flexible linker (exon 9), the transmembrane domain (exons 9 and 10), and the KASH motif (exon 10), two shorter splice isoforms exist: isoform A terminates just after the FHF domain (using the two residues and STOP encoded by the alternative exon 8), whereas isoform C skips exon 9

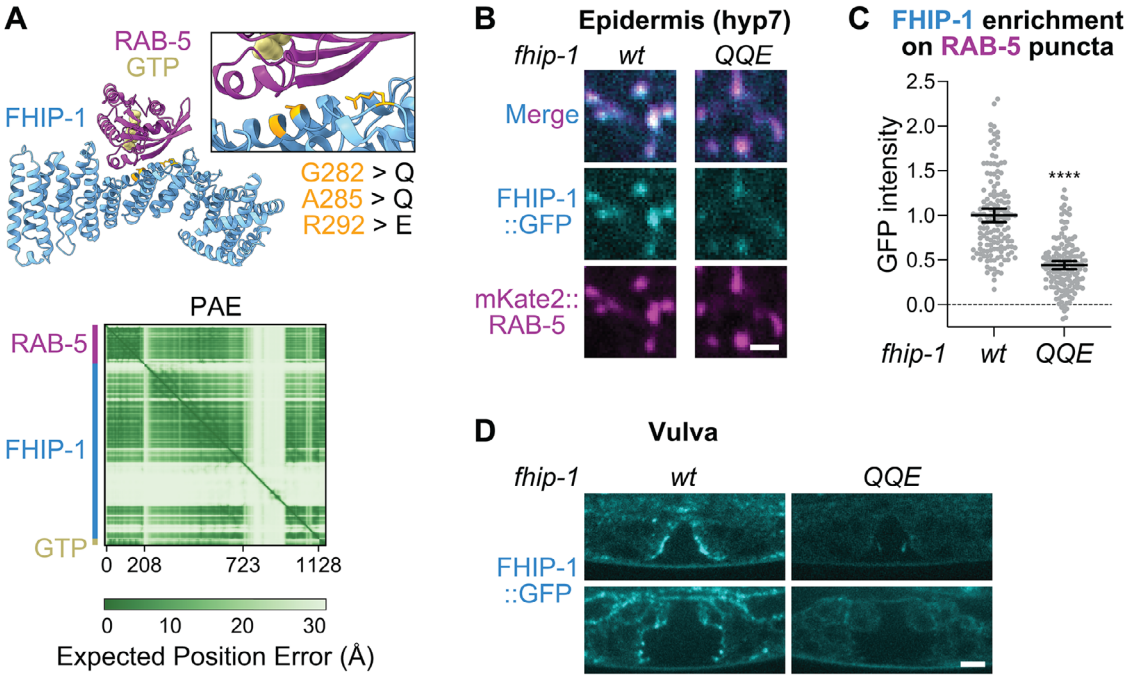

FIGURE 3: Structure prediction identifies residues in FHIP-1 important for recruitment to RAB-5. (A) AF3 model and Predicted Alignment Error (PAE) plot of FHIP-1 in complex with GTP-bound RAB-5. Full-length protein sequences were used for the prediction, but some disordered regions are not shown for clarity. In the PAE plot, aligned and scored residues are on the vertical and horizontal axis, respectively. Note that FHIP-1 has a large internal flexible loop, the start of which is marked in the PAE plot by residue 723. Three FHIP-1 residues at the RAB-5 binding interface and the mutations introduced by genome editing are highlighted. (B) Images of hyp7 in L4 animals coexpressing FHIP-1::GFP and transgenic mKate2::RAB-5. *wt*, wild-type. Scale bar, 2 µm. (C) FHIP-1::GFP intensity on mKate2::RAB-5 puncta in hyp7, quantified in images such as (B). Measurements of individual puncta from at least 10 animals are shown along with mean ± 95% CI (total number of puncta = 146 and 155 for *wt* and *QQE*, respectively). Statistical significance was determined by the Mann–Whitney test. ****$P < 0.0001$. CI, confidence interval. (D) Images of the early *(top)* and mid *(bottom)* L4 vulva in animals expressing FHIP-1::GFP. Similar localization was observed in at least 10 animals for each condition and developmental stage. Scale bar, 5 µm.

(Figure 5A). As a consequence, isoform C lacks the flexible linker, and the N-terminal six residues of its transmembrane domain are predicted to be encoded by exon 7, resulting in partial overlap between the transmembrane domain and the FHIP-1-binding helix at the C-terminus of the FHF domain (Figure 5A).

In prior work, expression of transgenic GFP::ZYG-12 was used to show that isoform A fails to localize to the NE but retains its ability to localize to centrosomes, while isoforms B and C localize to both the NE and centrosomes (Malone *et al.*, 2003). To address how splice isoforms contribute to EE recruitment of ZYG-12, we used genome editing to restrict isoform expression to isoforms B and C (exon 8 deletion, Δ*ex8*) or isoform C only (exon 8 and 9 deletion, Δ*ex8+9*) (Figure 5A). Immunoblotting confirmed robust overall expression of either mutant (Supplemental Figure S1E). In Δ*ex8* animals, GFP::ZYG-12 showed reduced recruitment to epidermal mKate2::RAB-5 puncta and was mostly absent from the vulva (Figure 5, B–D). This suggests that isoform A is the main isoform in the vulva and contributes to EE localization of ZYG-12 in the larval epidermis. In Δ*ex8+9* animals, GFP::ZYG-12 was strongly reduced at epidermal mKate2::RAB-5 puncta and completely absent from the vulva (Figure 5, B–D). By contrast, Δ*ex8+9* did not affect GFP::ZYG-12 recruitment to the NE or centrosomes (Figure 5E), and animals were fully viable and fertile (Supplemental Figure S1D). This demonstrates that isoform C is sufficient for ZYG-12 function at the NE and is likely the predominant isoform in the gonad and early embryo. Moreover, the difference in GFP::ZYG-12 intensity on mKate2::RAB-5 puncta between Δ*ex8* and Δ*ex8+9* shows that isoform B contributes to EE recruitment in the epidermis (Figure 5, B and C). In summary, our results suggest that isoform A targets exclusively to EE, isoform B targets to both EE and the NE, and isoform C targets exclusively to the NE (Figure 5F). We conclude that ZYG-12 recruitment to EE and the NE is regulated by alternative splicing of its C-terminal cargo binding domain.

DISCUSSION

Hook proteins constitute one of the most widely conserved family of dynein adaptors. In filamentous fungi, human cancer cells, and cultured rat neurons, Hook proteins have been shown to function as part of the FHF complex, which provides the link to membrane cargo by associating with small GTPases (Bielska *et al.*, 2014; Yao *et al.*, 2014; Zhang *et al.*, 2014; Guo *et al.*, 2016; Olenick *et al.*, 2019; Mattera *et al.*, 2020; Christensen *et al.*, 2021). Here, we show that the sole *C. elegans* Hook protein ZYG-12 has two distinct functions, only one of which involves FHF. In the larval epidermis and the developing vulva, ZYG-12 requires the FHIP homologue FHIP-1 to target to EE, a function which ZYG-12 shares with its fungal and vertebrate counterparts. By contrast, FHIP-1 is dispensable for ZYG-12's evolutionarily divergent function at the NE in the gonad and early embryo, first described two decades ago (Malone *et al.*, 2003). The *fhip-1(ko)* mutant demonstrates that FHF is not essential

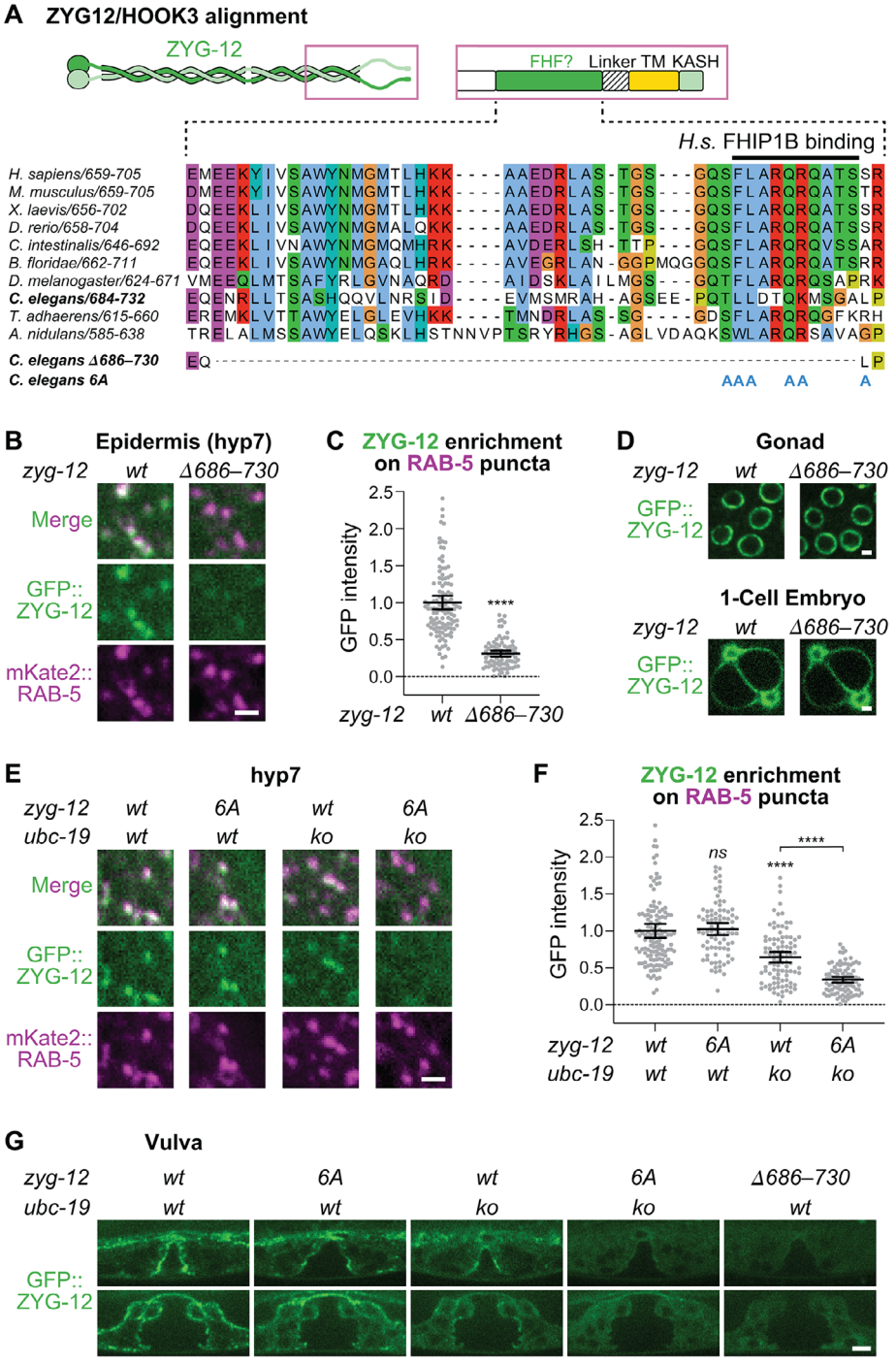

FIGURE 4: ZYG-12 recruitment to early endosomes and the nuclear envelope is mediated by distinct C-terminal domains. (A) Schematic of the ZYG-12 C-terminal domains *(top)* and sequence alignment with HOOK3 homologues *(bottom)*. The segment in human HOOK3 that binds FHIP1B is indicated above the alignment, and residues mutated in ZYG-12 to prevent binding to FHIP-1 (6A mutant) are indicated below. TM, transmembrane domain. (B, E) Images of hyp7 in L4 animals coexpressing GFP::ZYG-12 and transgenic mKate2::RAB-5. *wt*, wild-type; *ko*, knockout. Scale bars, 2 µm. (C, F) GFP::ZYG-12 intensity on mKate2::RAB-5 puncta in hyp7, quantified in images such as (B) and (E), respectively. Measurements of individual puncta from at least 10 animals are shown along with mean ± 95% CI (total number of puncta = 118 and 86 for *wt* and *Δ686–730*, respectively, in C; $n = 131$, 96, 97, and 93 for *wt/wt*, *6A/wt*, *wt/ko*, and *6A/ko*, respectively, in F). Statistical significance was determined by the Mann–Whitney test (C) or by ANOVA on ranks (Kruskal–Wallis nonparametric test) followed by Dunn's multiple comparison test (F). ****$P < 0.0001$; *ns* = not significant, $P > 0.05$. CI, confidence interval. (D) Images of GFP::ZYG-12 in the L4 meiotic gonad and one-cell embryo. Similar localization was observed in gonads and embryos of at least 10 animals for each condition. Scale bars, 2 µm. (G) Images of the early *(top)* and mid *(bottom)* L4 vulva in animals expressing GFP::ZYG-12. Similar localization was observed in at least 10 animals for each condition and developmental stage. Scale bar, 5 µm.

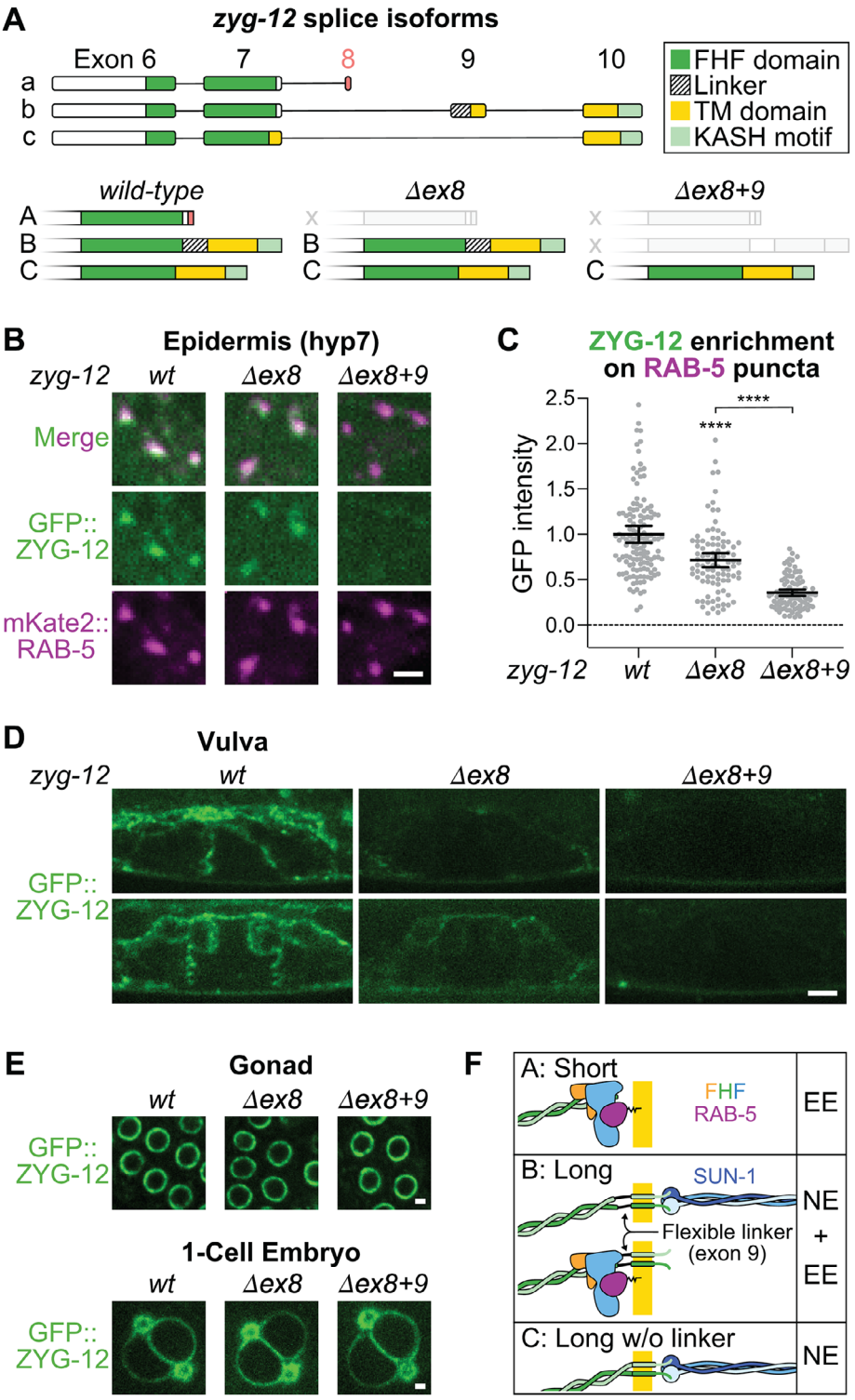

FIGURE 5: ZYG-12 recruitment to early endosomes and the nuclear envelope is regulated by C-terminal splicing. (A) Schematic of exons 6–10 of the *zyg-12* locus with the three (a,b,c) splice isoforms *(top)* and corresponding proteins *(bottom)*. The effect of deleting specific exons (Δ*ex*) on isoform expression is indicated. The transmembrane (TM) domain was predicted separately for each isoform using the SMART server (Simple Modular Architecture Research Tool; http://smart.embl-heidelberg.de/). Note that the N-terminal residues of the TM domain in isoforms B and C are encoded by different exons. (B) Images of hyp7 in L4 animals coexpressing GFP::ZYG-12 and transgenic mKate2::RAB-5. *wt*, wild-type. Scale bar, 2 μm. (C) GFP::ZYG-12 intensity on mKate2::RAB-5 puncta in hyp7, quantified in images such as (B). Measurements of individual puncta from at least 10 animals are shown along with mean ± 95% CI (total number of puncta = 131, 92, and 97 for *wt*, Δ*ex8*, and Δ*ex8+9*, respectively). Statistical significance was determined by ANOVA on ranks (Kruskal–Wallis nonparametric test) followed by Dunn's multiple comparison test. ****$P < 0.0001$. CI, confidence interval. (D) Images of the early *(top)* and mid *(bottom)* L4 vulva in animals expressing

for viability, and *fhip-1(ko)* animals are superficially normal, which contrasts with ZYG-12's critical LINC function at the NE and hints at additional pathways for EE positioning.

We mapped the region in ZYG-12 responsible for EE targeting (FHF domain) to residues 686–730, which agrees well with the recently determined structure of human FHF, in which the analogous region in HOOK3 associates with FTS and FHIP1B (Abid Ali *et al.*, 2025). Further functional dissection of FHF showed that ZYG-12 is still discernable at EE in the absence of the FTS homologue UBC-19, implying that ZYG-12 directly binds to FHIP-1. Mutation of a short ZYG-12 helix at the C-terminus of the FHF domain, predicted to mediate the only direct contact between ZYG-12 and FHIP-1 (and, respectively, between human HOOK3 and FHIP1B), did not affect EE targeting of ZYG-12, provided that UBC-19 was present. This suggests that the extensive FTS–FHIP and FTS–Hook contacts within FHF (Abid Ali *et al.*, 2025) can compensate for the absence of a direct Hook–FHIP interaction. Finally, we used structure prediction and mutagenesis to map the RAB-5 binding site on FHIP-1, which lies on the opposite side of the ZYG-12 and UBC-19 binding sites. Taken together, our functional characterization of FHF in vivo, using targeted mutagenesis and endogenously tagged subunits, suggests that FHIP-1 links ZYG-12 to RAB-5 and that UBC-19 stabilizes the FHIP-1–ZYG-12 interaction, in agreement with biochemical and structural analysis of fungal and human FHF (Xu *et al.*, 2008; Yao *et al.*, 2014; Mattera *et al.*, 2020; Christensen *et al.*, 2021; Abid Ali *et al.*, 2025). Our FHF mutants should be useful for examining the contribution of this conserved complex to the various membrane trafficking events in which Hook proteins have been implicated, including endocytic cargo sorting and endosome maturation (Krämer and Phistry, 1996, 1999; Sunio *et al.*, 1999; Ge *et al.*, 2010; Baron Gaillard *et al.*, 2011; Maldonado-Báez *et al.*, 2013; Bielska *et al.*, 2014).

ZYG-12's dual role as a dynein adaptor for two distinct membrane compartments parallels the multifunctionality of the Bicaudal D adaptor, which in case of vertebrate BICD2 recruits dynein to the NE and golgi-derived vesicles (Reck-Peterson *et al.*, 2018). In BICD2, the C-terminal binding sites for Nup358 (also called RanBP2) at the NE and Rab6 on vesicles show significant overlap, and the two components compete for binding (Gibson *et al.*, 2022, 2023; Zhao *et al.*, 2024). By contrast, the NE and EE targeting domains in ZYG-12 are distinct, which allows for regulation of cargo specificity by alternative splicing. The short isoform A terminates after the FHF domain, precluding its recruitment to the NE but still allowing centrosome targeting (Malone *et al.*, 2003). The long isoforms B and C only differ by a flexible linker, which in isoform B separates the FHF and transmembrane domains. Our gene editing experiments show that isoforms A and B are the predominant isoforms localized at EE in epithelia, and that isoform C is sufficient for LINC complex function at the NE in the gonad and early embryo. Taken together with prior analysis of isoform localization in the embryo (Malone *et al.*, 2003), these results suggest that isoform B is able to target to both the NE and EE, whereas isoform C is likely specialized for NE targeting. We speculate that the flexible linker in isoform B acts as a spacer, ensuring that FHF binding to RAB-5 and insertion of the ZYG-12 transmembrane domain into the EE lipid bilayer do not interfere with each other (Figure 5F). The presence of a bifunctional isoform B, alongside the organelle-specific isoforms A and C, suggests that during certain stages of development ZYG-12 may recruit dynein to the NE and EE within the same cell type. Our findings highlight alternative splicing of adaptors as a mechanism for tissue-specific regulation of dynein–cargo interactions.

MATERIALS AND METHODS

Request a protocol through *Bio-protocol*

C. elegans strains

Strains (Supplemental Table S1) were maintained at 20°C on standard nematode growth media (NGM) plates seeded with OP50 bacteria. CRISPR/Cas9-mediated genome editing (Supplemental Table S2) was performed as described (Arribere *et al.*, 2014; Paix *et al.*, 2014; Dokshin *et al.*, 2018) using crRNAs (Integrated DNA Technologies), home-made Cas9 protein, and a repair template consisting of an oligonucleotide (Integrated DNA Technologies), a gBlock (Integrated DNA Technologies), or a partially single-stranded PCR product (Dokshin *et al.*, 2018). All edits were confirmed by sequencing.

A Mos1 transposon-based strategy (Frøkjaer-Jensen *et al.*, 2012) was used to generate strains expressing transgenic mKate2::RAB-5 (*prtSi260*) and CTNS-1::mKate2 (*prtSi261*) in the epidermis from the *dpy-7* promoter (1.38 kb), and mKate2::RAB-5 (*prtSi294*) in the vulva from the *nmy-1* promoter (3.16 kb). Expression cassettes were cloned into pCFJ151 for insertion on chromosome V (oxTi365).

Embryonic viability and brood size

Brood size and embryonic viability assays were performed at 20°C. L4 hermaphrodites were grown for 40 h on NGM plates containing OP50 bacteria. Single adults were then placed on new plates with a small amount of OP50, removed 6 h later, and the plates were incubated for another 18 h to give viable embryos time to hatch. Embryonic viability was calculated by dividing the number of hatched larvae by the total number of progeny on the plate.

Fluorescence microscopy

For imaging of the epidermis, gonad, and vulva, hermaphrodites at the L4 stage (or L3 stage for Supplemental Figure S3) were immobilized with 5 mM levamisole for 10 min. For imaging of embryos, gravid adults were dissected in M9 buffer (86 mM NaCl, 42 mM Na_2HPO_4, 22 mM KH_2PO_4, 1 mM $MgSO_4$). Animals or embryos were then mounted on a freshly prepared 2% (wt/vol) agarose pad and covered with an 18 mm × 18 mm coverslip (No. 1.5H, Marienfeld). Imaging was performed at 20°C on a Nikon Eclipse Ti microscope coupled to an Andor Revolution XD spinning disk confocal system, composed of an iXon Ultra 897 CCD camera (Andor Technology), a solid-state laser combiner (ALC-UVP 350i, Andor Technology), and a CSU-X1 confocal scanner (Yokogawa Electric Corporation), controlled by IQ3 software (Andor Technology). A 60× NA 1.4 Plan-Apochromat objective was used to acquire z-stacks of 3.4 µm (step size 0.2 µm), 12.4 µm (step size 0.18 µm) and 7 µm (step size 1 µm) for the epidermis, vulva, and embryos, respectively. A 100× NA 1.45 Plan-Apochromat objective was used to acquire a z-stack of 6.7 µm (step size 0.18 µm) for VPCs. For time-lapse imaging of mCherry::RAB-5 in embryos, images were acquired with the

GFP::ZYG-12. Similar localization was observed in at least 10 animals for each condition and developmental stage. Scale bar, 5 µm. (E) Images of GFP::ZYG-12 in the L4 meiotic gonad and one-cell embryo. Similar localization was observed in gonads and embryos of at least 10 animals for each condition. Scale bars, 2 µm. (F) Summary of the proposed endomembrane targeting capacities of the three ZYG-12 isoforms.

60× objective at 2 frames per second in a single z-plane such that the centrosomes were in focus.

Image analysis

Image analysis was performed on unprojected z-stack images using Fiji software. To quantify the signal intensity of puncta in the hyp7 syncytium of L4 animals (Figures 1E, 2D, 3C, 4, C and F, 5C), two circles, differing in radius by 1 pixel, were drawn around well-isolated puncta of GFP::ZYG-12 (for mCh::DHC-1 measurements) or mKate2::RAB-5 (for GFP::ZYG-12 or FHIP-1::GFP measurements). The integrated fluorescence intensity of the region between the two circles was considered background and was subtracted from the integrated fluorescence intensity of the inner circle after normalization to the inner circle area. To quantify EE distribution in VPCs of L3 animals (Supplemental Figure S3B), a straight line with a thickness approximately corresponding to the nuclear diameter was drawn along the apical-basal axis, and intensity values along the line were recorded using the Plot Profile function. Individual line scan profiles were aligned relative to the apical peak, and intensity values were normalized to the average intensity of the apical peak in controls. Images in figures correspond to single z-sections. Images of controls and mutants were scaled equally for brightness and contrast.

Immunoblotting

Freshly starved mixed-stage animals were washed with M9 buffer (42 mM Na_2HPO_4, 22 mM KH_2PO_4, 1 mM $MgSO_4$, 86 mM NaCl) from a 60-mm petri dish into a 15-ml conical, pelleted for 5 min at 4000 rcf, transferred into a 1.5-ml tube, and washed again with 3 × 1 ml M9 buffer. To 100 µl of worm suspension, 33 µl 4× SDS–PAGE sample buffer (200 mM Tris-HCl pH 6.8, 40% [vol/vol] glycerol, 8% [wt/vol] SDS, 400 mM DTT, 0.4% [wt/vol] bromophenol blue) and ~20 µl of glass beads were added. Samples were incubated for 3 min at 95°C, vortexed for 2 × 5 min, and clarified at 20,000 rcf for 1 min at room temperature. A total of 10 µl of supernatant were resolved by 10% SDS–PAGE and proteins were transferred to 0.2-µm nitrocellulose membranes (GE Healthcare). Membranes were blocked with 5% nonfat dry milk in TBS-T (20 mM Tris-HCl pH 7.5, 140 mM NaCl, 0.2% [vol/vol] Tween 20) for 1 h and probed overnight at 4°C with rabbit polyclonal anti-GFP (OD158; 1:3000) and mouse monoclonal anti-α-tubulin antibody (clone B-5-1-2; Merck T5168; 1:5000). Membranes were washed 4 × 7 min with TBS-T and incubated for 1 h at room temperature in 5% nonfat dry milk/TBS-T containing goat polyclonal anti-rabbit IgG (111-035-003) and anti-mouse IgG (115-035-003) coupled to horseradish peroxidase (Jackson ImmunoResearch; 1:10,000). Membranes were washed again 4 × 7 min with TBS-T and incubated with Clarity Western ECL Substrate (Bio-Rad). Proteins were visualized using the Bio-Rad ChemiDoc XRS+ system controlled by Image Lab software.

Structure prediction

AlphaFold 3 (Abramson *et al.*, 2024) was used for structure prediction (alphafoldserver.com). The input for the GTP–RAB-5–FHIP-1 complex (Figure 3A) consisted of one copy each of full-length C05D11.8/FHIP-1 (UniProt Q11187), full-length RAB-5 (UniProt P91857), and GTP ligand. The input for the GTP–RAB-5–FHF complex (Supplemental Figure S2A) additionally consisted of one copy of full-length UBC-19 (UniProt Q9U1U4) and two copies of ZYG-12 residues 649–736 (UniProt Q23529-2). The input for the FHIP-1–ZYG-12 helix complex (Supplemental Figure S2B) consisted of one copy of FHIP-1 residues 275–523, one copy of FHIP-1 residues 749–920, and one copy of ZYG-12 residues 714–736. Structures were visualized with UCSF ChimeraX (Pettersen *et al.*, 2021).

Statistical analysis

Statistical analysis was performed with Prism 10.0 software (GraphPad). Statistical significance was determined by the Mann–Whitney test or by ANOVA on ranks (Kruskal–Wallis nonparametric test) followed by Dunn's multiple comparison test, where $****P < 0.0001$, $***P < 0.001$, $**P < 0.01$, $*P < 0.05$, and *ns* = not significant, $P > 0.05$. The analytical method used is specified in the figure legends.

ACKNOWLEDGMENTS

This project was funded by the Fundação para a Ciência e a Tecnologia (FCT)/Ministério da Ciência, Tecnologia e Ensino Superior (PTDC/BIA-CEL/1321/2021). R.G. and A.X.C. were supported by FCT Principal Investigator positions (CEECIND/00333/2017 and CEECIND/01967/2017, respectively), D.J.B. and F.-Y.C. were supported by FCT Junior Researcher positions (DL57/2016/CP1355/CT0007 and DL57/2016/CP1355/CT0013, respectively), and C.C. was supported by an FCT PhD fellowship (SFRH/BD/144877/2019). M.G. and D.K.C. were supported by a Sir Henry Dale Fellowship to D.K.C. jointly funded by the Wellcome Trust and the Royal Society (208833/Z/17/Z). The authors acknowledge WormBase (Davis *et al.*, 2022) for providing data and tools. Some strains were provided by the Caenorhabditis Genetics Center (CGC), which is funded by the NIH Office of Research Infrastructure Programs (P40 OD010440). UCSF ChimeraX is developed by the Resource for Biocomputing, Visualization, and Informatics at the University of California, San Francisco, with support from National Institutes of Health R01-GM129325 and the Office of Cyber Infrastructure and Computational Biology, National Institute of Allergy and Infectious Diseases.

REFERENCES

Abid Ali F, Zwetsloot AJ, Stone CE, Morgan TE, Wademan RF, Carter AP, Straube A (2025). KIF1C activates and extends dynein movement through the FHF cargo adapter. Nat Struct Mol Biol. https://doi.org/10.1038/s41594-024-01418-z.

Abramson J, Adler J, Dunger J, Evans R, Green T, Pritzel A, Ronneberger O, Willmore L, Ballard AJ, Bambrick J, *et al.* (2024). Accurate structure prediction of biomolecular interactions with AlphaFold 3. Nature 630, 493–500.

Arribere JA, Bell RT, Fu BX, Artiles KL, Hartman PS, Fire AZ (2014). Efficient marker-free recovery of custom genetic modifications with CRISPR/Cas9 in *Caenorhabditis elegans*. Genetics 198, 837–846.

Barbosa DJ, Duro J, Prevo B, Cheerambathur DK, Carvalho AX, Gassmann R (2017). Dynactin binding to tyrosinated microtubules promotes centrosome centration in *C. elegans* by enhancing dynein-mediated organelle transport. PLoS Genet 13, e1006941.

Baron Gaillard CL, Pallesi-Pocachard E, Massey-Harroche D, Richard F, Arsanto J-P, Chauvin J-P, Lecine P, Krämer H, Borg J-P, Le Bivic A (2011). Hook2 is involved in the morphogenesis of the primary cilium. Mol Biol Cell 22, 4549–4562.

Bielska E, Schuster M, Roger Y, Berepiki A, Soanes DM, Talbot NJ, Steinberg G (2014). Hook is an adapter that coordinates kinesin-3 and dynein cargo attachment on early endosomes. J Cell Biol 204, 989–1007.

Carter AP, Diamant AG, Urnavicius L (2016). How dynein and dynactin transport cargos: A structural perspective. Curr Opin Struct Biol 37, 62–70.

Celestino R, Henen MA, Gama JB, Carvalho C, McCabe M, Barbosa DJ, Born A, Nichols PJ, Carvalho AX, Gassmann R, *et al.* (2019). A transient helix in the disordered region of dynein light intermediate chain links the motor to structurally diverse adaptors for cargo transport. PLoS Biol 17, e3000100.

Christensen JR, Kendrick AA, Truong JB, Aguilar-Maldonado A, Adani V, Dzieciatkowska M, Reck-Peterson SL (2021). Cytoplasmic dynein-1 cargo diversity is mediated by the combinatorial assembly of FTS–Hook–FHIP complexes. Elife 10, e74538.

Davis P, Zarowiecki M, Arnaboldi V, Becerra A, Cain S, Chan J, Chen WJ, Cho J, da Veiga Beltrame E, Diamantakis S, *et al*. (2022). WormBase in 2022–data, processes, and tools for analyzing *Caenorhabditis elegans*. Genetics 220, iyac003.

Dokshin GA, Ghanta KS, Piscopo KM, Mello CC (2018). Robust genome editing with short single-stranded and long, partially single-stranded DNA donors in *Caenorhabditis elegans*. Genetics 210, 781–787.

Frøkjaer-Jensen C, Davis MW, Ailion M, Jorgensen EM (2012). Improved Mos1-mediated transgenesis in *C. elegans*. Nat Methods 9, 117–118.

Ge X, Frank CL, Calderon de Anda F, Tsai L-H (2010). Hook3 interacts with PCM1 to regulate pericentriolar material assembly and the timing of neurogenesis. Neuron 65, 191–203.

Gibson JM, Cui H, Ali MY, Zhao X, Debler EW, Zhao J, Trybus KM, Solmaz SR, Wang C (2022). Coil-to-α-helix transition at the Nup358-BicD2 interface activates BicD2 for dynein recruitment. Elife 11, e74714.

Gibson JM, Zhao X, Ali MY, Solmaz SR, Wang C (2023). A structural model for the core Nup358-BicD2 interface. Biomolecules 13, 1445.

Guo X, Farías GG, Mattera R, Bonifacino JS (2016). Rab5 and its effector FHF contribute to neuronal polarity through dynein-dependent retrieval of somatodendritic proteins from the axon. Proc Natl Acad Sci U S A 113, E5318–E5327.

Kimura K, Kimura A (2011). Intracellular organelles mediate cytoplasmic pulling force for centrosome centration in the *Caenorhabditis elegans* early embryo. Proc Natl Acad Sci U S A 108, 137–142.

Krämer H, Phistry M (1996). Mutations in the *Drosophila* hook gene inhibit endocytosis of the boss transmembrane ligand into multivesicular bodies. J Cell Biol 133, 1205–1215.

Krämer H, Phistry M (1999). Genetic analysis of hook, a gene required for endocytic trafficking in *Drosophila*. Genetics 151, 675–684.

Lee I-G, Olenick MA, Boczkowska M, Franzini-Armstrong C, Holzbaur ELF, Dominguez R (2018). A conserved interaction of the dynein light intermediate chain with dynein–dynactin effectors necessary for processivity. Nat Commun 9, 986.

Maheshwari R, Rahman MM, Drey S, Onyundo M, Fabig G, Martinez MAQ, Matus DQ, Müller-Reichert T, Cohen-Fix O (2023). A membrane reticulum, the centriculum, affects centrosome size and function in *Caenorhabditis elegans*. Curr Biol 33, 791–806.e7.

Maldonado-Báez L, Cole NB, Krämer H, Donaldson JG (2013). Microtubule-dependent endosomal sorting of clathrin-independent cargo by Hook1. J Cell Biol 201, 233–247.

Malone CJ, Misner L, Bot NL, Tsai M-C, Campbell JM, Ahringer J, White JG (2003). The *C. elegans* hook protein, ZYG-12, mediates the essential attachment between the centrosome and nucleus. Cell 115, 825–836.

Mattera R, Williamson CD, Ren X, Bonifacino JS (2020). The FTS-Hook-FHIP (FHF) complex interacts with AP-4 to mediate perinuclear distribution of AP-4 and its cargo ATG9A. Mol Biol Cell 31, 963–979.

Meyerzon M, Gao Z, Liu J, Wu J-C, Malone CJ, Starr DA (2009). Centrosome attachment to the *C. elegans* male pronucleus is dependent on the surface area of the nuclear envelope. Dev Biol 327, 433–446.

Minn IL, Rolls MM, Hanna-Rose W, Malone CJ (2009). SUN-1 and ZYG-12, mediators of centrosome-nucleus attachment, are a functional SUN/KASH pair in *Caenorhabditis elegans*. Mol Biol Cell 20, 4586–4595.

Olenick A, Dominguez R, Holzbaur ELF (2019). Dynein activator Hook1 is required for trafficking of BDNF-signaling endosomes in neurons. J Cell Biol 218, 220–233.

Paix A, Wang Y, Smith HE, Lee C-YS, Calidas D, Lu T, Smith J, Schmidt H, Krause MW, Seydoux G (2014). Scalable and versatile genome editing using linear DNAs with microhomology to Cas9 sites in *Caenorhabditis elegans*. Genetics 198, 1347–1356.

Penkner A, Tang L, Novatchkova M, Ladurner M, Fridkin A, Gruenbaum Y, Schweizer D, Loidl J, Jantsch V (2007). The nuclear envelope protein Matefin/SUN-1 is required for homologous pairing in *C. elegans* meiosis. Dev Cell 12, 873–885.

Penkner AM, Fridkin A, Gloggnitzer J, Baudrimont A, Machacek T, Woglar A, Csaszar E, Pasierbek P, Ammerer G, Gruenbaum Y, *et al*. (2009). Meiotic chromosome homology search involves modifications of the nuclear envelope protein Matefin/SUN-1. Cell 139, 920–933.

Pettersen EF, Goddard TD, Huang CC, Meng EC, Couch GS, Croll TI, Morris JH, Ferrin TE (2021). UCSF ChimeraX: Structure visualization for researchers, educators, and developers. Protein Sci 30, 70–82.

Reck-Peterson SL, Redwine WB, Vale RD, Carter AP (2018). The cytoplasmic dynein transport machinery and its many cargoes. Nat Rev Mol Cell Biol 19, 382–398.

Sato A, Isaac B, Phillips CM, Rillo R, Carlton PM, Wynne DJ, Kasad RA, Dernburg AF (2009). Cytoskeletal forces span the nuclear envelope to coordinate meiotic chromosome pairing and synapsis. Cell 139, 907–919.

Sunio A, Metcalf AB, Krämer H (1999). Genetic dissection of endocytic trafficking in *Drosophila* using a horseradish peroxidase-bride of sevenless chimera: Hook is required for normal maturation of multivesicular endosomes. Mol Biol Cell 10, 847–859.

Walenta JH, Didier AJ, Liu X, Krämer H (2001). The golgi-associated Hook3 protein is a member of a novel family of microtubule-binding proteins. J Cell Biol 152, 923–934.

Wang J, Chitsaz F, Derbyshire MK, Gonzales NR, Gwadz M, Lu S, Marchler GH, Song JS, Thanki N, Yamashita RA, *et al*. (2022). The conserved domain database in 2023. Nucleic Acids Res 51, D384–D388.

Xu L, Sowa ME, Chen J, Li X, Gygi SP, Harper JW (2008). An FTS/Hook/p107(FHIP) complex interacts with and promotes endosomal clustering by the homotypic vacuolar protein sorting complex. Mol Biol Cell 19, 5059–5071.

Yao X, Wang X, Xiang X (2014). FHIP and FTS proteins are critical for dynein-mediated transport of early endosomes in *Aspergillus*. Mol Biol Cell 25, 2181–2189.

Zhang J, Qiu R, Arst HN, Peñalva MA, Xiang X (2014). HookA is a novel dynein–early endosome linker critical for cargo movement in vivo. J Cell Biol 204, 1009–1026.

Zhao X, Quintremil S, Castro EDR, Cui H, Moraga D, Wang T, Vallee RB, Solmaz SR (2024). Molecular mechanism for recognition of the cargo adapter Rab6^{GTP} by the dynein adapter BicD2. Life Sci Alliance 7, e202302430.

Zhou K, Rolls MM, Hall DH, Malone CJ, Hanna-Rose W (2009). A ZYG-12-dynein interaction at the nuclear envelope defines cytoskeletal architecture in the *C. elegans* gonad. J Cell Biol 186, 229–241.